

Bone marrow mesenchymal stem cell-derived exosomal miR-30e-5p ameliorates high-glucose induced renal proximal tubular cell pyroptosis by inhibiting ELAVL1

Jia Lv, Ya-Ning Hao, Xiao-Pei Wang, Wan-Hong Lu, Li-Yi Xie and Dan Niu

Department of Nephrology, College of Medicine, Nephrotic Hospital, First Affiliated Hospital, Xi'an Jiaotong University, Xi'an, PR China

ABSTRACT

Background: The rapid increase in the prevalence of diabetes has resulted in more cases of diabetic kidney disease (DKD). Treatment with bone marrow mesenchymal stem cells (BMSCs) may represent an alternative strategy to manage DKD.

Methods: HK-2 cells were treated with 30 mM high glucose (HG). Bone marrow MSC-derived exosomes (BMSC-exos) were isolated and internalized into HK-2 cells. 3-(4,5-Dimethylthiazol-2-yl)-2,5-diphenyltetrazoliumbromide (MTT) and lactate dehydrogenase (LDH) assays were used to measure viability and cytotoxicity. The secretion of IL-1 β and IL-18 was measured by ELISA. Pyroptosis was assessed by flow cytometry. Quantitative RT-PCR was used to measure the levels of miR-30e-5p, ELAV like RNA binding protein 1 (ELAVL1), IL-1 β , and IL-18. The expression of ELAVL1 and pyroptosis-associated cytokine proteins was determined by western blot analysis. A dual-luciferase reporter gene assay was conducted to confirm the relationship between miR-30e-5p and ELAVL1.

Results: BMSC-exos decreased LDH, IL-1 β , and IL-18 secretion and inhibited the expression of the pyroptosis-related factors (IL-1 β , caspase-1, GSDMD-N, and NLRP3) in HG-induced HK-2 cells. Moreover, miR-30e-5p depletion derived from BMSC-exos promoted HK-2 cell pyroptosis. Besides, miR-30e-5p over-expression or ELVAL1 knockdown could directly inhibit pyroptosis. ELAVL1 was a target of miR-30e-5p and knocking down ELAVL1 reversed the effect of miR-30e-5p inhibition in BMSC-exos-treated HK-2 cells.

Conclusions: BMSC-derived exosomal miR-30e-5p inhibits caspase-1-mediated pyroptosis by targeting ELAVL1 in HG-induced HK-2 cells, which might provide a new strategy for treating DKD.

ARTICLE HISTORY

Received 6 July 2022
Revised 31 January 2023
Accepted 31 January 2023

KEYWORDS

Pyroptosis; bone marrow mesenchymal stem cells; exosome; miR-30e-5p; diabetic kidney disease

1. Introduction

Diabetic kidney disease (DKD) can cause chronic kidney disease. DKD is associated with albuminuria, progressive loss of kidney function, glomerular hypertrophy, and renal fibrosis [1,2]. The conventional treatment for DKD is effective in the early stages of renal damage, but not at an advanced stage, in which hyperglycemia and hypertension occur [3]. Dialysis and kidney transplantation are also helpful in treating kidney failure, but immune system rejection and a lack of donors are the primary limitation for their overall success [4]. Therefore, it is necessary to identify the mechanism of DKD in detail to develop new treatment strategies.

With the development of stem cell therapy, mesenchymal stem cells (MSCs) have gained interest as a

potential therapy for renal damage [5]. MSCs exhibit a self-renewal capacity and multilineage differentiation potential [3]. Bone marrow, adipose tissue, and umbilical cord are the primary sources of MSCs. MSCs have protective effects against diabetic retinopathy, myocardial infarction, diabetes, and DKD [4,6–8]. In addition, MSCs can secrete cytokines, chemokines, growth factors, and extracellular vesicles [9]. Exosomes, which are a type of extracellular vesicle, range in size from 30 to 150 nm and are ubiquitous in body fluid. The underlying mechanism of bone marrow MSC-derived exosomes (BMSC-exos) may involve their function as mediators of intercellular communication and immune regulation [10,11].

Exosomes contain mRNAs, microRNAs (miRNA), and proteins. miRNAs are small noncoding transcripts that

CONTACT Dan Niu  niudan604@126.com  Department of Nephrology, College of Medicine, Nephrotic Hospital, First Affiliated Hospital, Xi'an Jiaotong University, No. 277 Yanta Road, Xi'an 710061, Shanxi Province, PR China

 Supplemental data for this article can be accessed online at <https://doi.org/10.1080/0886022X.2023.2177082>

© 2023 The Author(s). Published by Informa UK Limited, trading as Taylor & Francis Group.

This is an Open Access article distributed under the terms of the Creative Commons Attribution License (<http://creativecommons.org/licenses/by/4.0/>), which permits unrestricted use, distribution, and reproduction in any medium, provided the original work is properly cited.

can regulate cell proliferation, apoptosis, oxidative stress, inflammatory factors, as well as other functions and participate in the occurrence and development of tumors, diabetes, Parkinson's disease, and other diseases [12]. Recently, the effects of miRNAs on kidney disease have attracted attention. Thus far, miRNA dysregulation was shown to cause DKD, indicating that miRNAs may be useful diagnostic biomarkers for DKD [13]. miR-30e-5p expression was dysregulated in liver carcinoma, chronic myeloid leukemia, lung adenocarcinoma, colorectal cancer, and type 1 diabetes [14–17]. In addition, miR-30e-5p was predicted to be highly expressed in BMSC-exos; however, it was down-regulated in DKD [18]. Thus, we hypothesized that miR-30e-5p may be effective in regulating HG induced renal tubular epithelial cell injury.

Pyroptosis refers to the process of pro-inflammatory programmed cell death [19]. The NOD-like receptor pyrin containing receptor 3 (NLRP3) inflammasome, ELAV-like RNA binding protein 1 (ELAVL1), and caspase-1 can promote the secretion of inflammatory cytokines and cause plasma membrane rupture, which are considered hallmark features of pyroptosis [20,21]. Moreover, ELAVL1 could be targeted by miR-23c to regulate HG induced renal tubular epithelial pyroptosis [22]. HuR, a member of the ELAV protein family, contributes to ischemia, renal fibrosis, matrix protein accumulation, and angiogenesis. Furthermore, HuR was found to be up-regulated in DKD patients; thus, HuR may play an important role in the pathogenesis of DKD [23]. It was proved that pyroptosis participated in the process of DKD and NLRP3 inflammasomes promoted DKD progression [24,25]. The starBase database (<http://starbase.sysu.edu.cn>) predicted that ELAVL1 may be a downstream target gene of miR-30e-5p, but such a relationship has not yet been reported.

In the present study, we hypothesized that bone marrow mesenchymal stem cell (BMSC)-derived exosomal miR-30e-5p ameliorates HG-induced HK-2 cell pyroptosis by targeting ELAVL1. Our findings may provide a new strategy for the treatment of DKD.

2. Materials and methods

2.1. Cell culture and drug treatment

HK-2 (human renal proximal tubular cells) cells were obtained from the American Type Culture Collection (Manassas, VA). The cells were cultured in RPMI 1640 media containing 10% FBS, hydrocortisone (5 ng/ml), glutamine (2 mM), sodium selenite (5 ng/ml), insulin (5 µg/ml), transferrin (5 µg/ml), penicillin (100 U/ml), and streptomycin (100 µg/ml) in 5% CO₂/95% humidified air

at 37 °C. To simulate a DKD model *in vitro*, 30 mM glucose was added for 72 h to establish the HG model, whereas 5.5 mM glucose was added as a normal (NG) control and an additional 24.5 mM mannitol was added as an isotonic control [17].

2.2. Preparation and characterization of BMSC-exos

BMSC-exos were obtained from the supernatant of human-BMSCs and collected at a density of 1.0×10^5 cells/well in a six-well plate. They were centrifuged at $2000 \times g$ for 20 min. The conditioned medium was ultracentrifuged at $100,000 \times g$. Exosomes were washed once with 4-(2-hydroxyethyl)-1-piperazineethanesulfonic acid (HEPES) (Sigma-Aldrich, St. Louis, MO) and the above procedure was repeated. The exosomes were resuspended in PBS, filtered, and stored at -80°C . Transmission electron microscopy was used to detect the presence of BMSC-exos and the particle sizes were assessed by nano-particle tracking analysis (NTA). The surface markers CD73, CD90, CD105, CD34, CD14, and CD45 were detected by Fluorescence-activated Cell Sorting (FACS) analysis. The surface markers CD63 and TSG101 were also analyzed by western blot analysis. Exosomes (100 µg/ml) were tagged with PKH67, a fluorescent linker dye (Sigma-Aldrich, St. Louis, MO), to trace them within cells. Finally, 30 µg BMSC-exos were added to HK-2 cells to determine their effect [26].

2.3. Internalization of BMSC-exos in HK-2 cells

BMSC-exos were labeled with the PKH67 membrane dye and 100 µg/ml were added to 3×10^4 HK-2. The cells were then washed with PBS and fixed with paraformaldehyde. The nucleus was counterstained with DAPI (1:200) and observed by fluorescence microscopy (Nikon, Tokyo, Japan) [27].

2.4. 3-(4,5-Dimethylthiazol-2-yl)-2,5-diphenyltetrazoliumbromide (MTT) assay

Cells were seeded into 96-well plates at a density of 2000 cells per well. After a 24-h incubation, the medium was removed and MTT (5 mg/ml, M2003, Sigma-Aldrich, St. Louis, MO) was added to each well. After 3 h, the MTT was removed and 200 µl of DMSO were added to each well. The absorbance was measured at 490 nm using a microplate reader (Tecan, Mannedorf, Switzerland).

2.5. Flow cytometry

HK-2 cells were plated in a six-well plate at a density of 2×10^5 cells per well. After 48 h, the cells were harvested, washed with PBS, and centrifuged at 1500 rpm for 5 min. FAM-YVAD-FMK (FAM600-1, Cell Technology, Hayward, CA), caspase-1 antibody, and propidium iodide were added to the resuspended cells and mixed. After incubating at room temperature in the dark for 1 h, the cells were analyzed using a BD Biosciences FACS Calibur system (San Jose, CA).

2.6. Cell transfection

The miR-30e-5p inhibitor (5'-CUUCCAGUCAAGGAUGUUUACA-3') and negative control (inhibitor NC, 5'-CAGUACUUUUGUGUAGUACAA-3'), miR-30e-5p mimics (sense: 5'-UGUAAACAUCUUGACUGGAAG-3', anti-sense: 5'-CUUCCAGUCAAGGAUGUUUACA-3') and negative control (mimics NC, sense: 5'-UUCUCCGAACGUGUCACGUTT-3', anti-sense: 5'-ACGUGACACGUUCGGAGAATT-3') and shRNA sequence targeting ELVAL1 (shELVAL1, 5'-CGTGGATCAGACTACAGGTTT-3') and negative control (shNC, 5'-GTTCTCCGAACGTGTACCGT-3') were synthesized by GenePharma (Shanghai, China). Lipofectamine 2000 (Thermo Fisher, Waltham, MA) was used for plasmid and siRNAs transfection. After 48–72 h transfection, the cells were harvested for additional assays.

2.7. Dual-luciferase reporter gene assay

Cell transfection was done as described above. Briefly, ELAVL1 3'-UTRs containing miR-30e-5p binding sites (ELAVL1-WT: 5'-GUUUAC-3') and its mutant (ELAVL1-MUT: 5'-CAAAUG-3') were constructed and cloned into the pGL3 vector. The recombinant luciferase vector and mimics-miR-30e-5p/mimics NC were co-transfected into HK-2 cells. Renilla luciferase was used as an internal control. Luciferase activity was measured following the instructions of the dual-luciferase reporter kit (Promega, Madison, WI).

2.8. ELISA assay

The IL-1 β and IL-18 levels in the supernatant fluid of HK-2 cells was measured using commercial kits according to the instructions. IL-1 β (product codes: H002; detection range: 0.5–100 ng/l; inter-batch difference rate: CV < 10%; intra-batch difference rate: CV < 12%); IL-18 (product codes: H015; detection range: 1–300 ng/l; inter-batch difference rate: CV < 10%; intra-batch difference rate: CV < 12%). The absorbance at 450 nm was

measured with a microplate reader (Thermo Fisher Scientific Inc., Waltham, MA).

2.9. Measurement of lactate dehydrogenase (LDH) level

Cells (1×10^6) were seeded into six-well cell culture plates for 12 h and after treatment, the cell supernatant was collected. LDH levels were measured using an LDH assay kit (C0016, Beyotime, Shanghai, China) based on the manufacturer's instructions. The absorbance was detected at 490 nm using a microplate reader (Thermo Fisher Scientific Inc., Waltham, MA).

2.10. qRT-PCR analysis

Total RNA was isolated using Trizol reagent (15596018, Ambion, Austin, TX) and stored at -80°C for further detection. For mRNA analysis, cDNA was synthesized using the SuperScriptTM IV First-Strand Synthesis System (6210A, Takara, Otsu, Japan), and qPCR was done using SYBR Green PCR Mastermix (SR1110, Solarbio, Beijing, China). For miRNA analysis, cDNA was synthesized using the Hairpin-itTM Real-Time PCR kit (E22001, GenePharma, Shanghai, China), which was analyzed using the corresponding U6 snRNA Normalization RT-qPCR Quantification Kit (E20001, GenePharma, Shanghai, China). GAPDH was served as internal reference for mRNA analysis and U6 served as internal reference for miRNA analysis. Data were analyzed using by the $2^{-\Delta\Delta\text{Ct}}$ method. The primer sequences are listed in Table 1.

2.11. Western blot analysis

Total protein extracts from HK-2 cells following various treatments were prepared in RIPA buffer containing protease inhibitors. The protein concentration was measured using a BCA assay kit (P0009, Beyotime, Shanghai, China). Thirty micrograms protein samples were separated by 12% sodium dodecyl sulfate-polyacrylamide gel electrophoresis (SDS-PAGE) and transferred to polyvinylidene fluoride membranes (Cytiva, Boston, MA). The membranes were blocked in TBS buffer containing 5% skim milk for 1 h and incubated with primary antibodies at 4°C overnight. The membranes were washed with TBST and incubated with the corresponding secondary antibody for 1 h. The signal was detected using an ECL Kit (Thermo Fisher, Waltham, MA). Anti-CD63 (ab134045), anti-TSG101 (ab133586), anti-ELAVL1 (ab200342), anti-IL-1 β (ab254360), anti-cleaved N-terminal domain of gasdermin D (GSDMD-N,

Table 1. Primer information.

	Forward primers	Reverse primers
IL-1 β	5'-CCCAAAGTGGAGATGAAAA-3'	5'-GGGTACAGGGCAGATTCAAA-3'
IL-18	5'-TGGCTGCTGAACCAGTAGAA-3'	5'-ATAGAGGCCGATTCCTTGG-3'
miR-30e-5p	5'-GGGTGTAACATCCTTGAC-3'	5'-TGCCTGCTGGAGTC-3'
ELAVL1	5'-GAGGCTCCAGTCAAAAACCA-3'	5'-GTTGGCGCTTTGATCACCT-3'
PFKFB2	5'-AGTCCTACGACTTCTTCGGC-3'	5'-TCTCCTCAGTGAGATACGCCT-3'
MAT2B	5'-ACAGAGAGGAAGACATACCAG-3'	5'-GTTTCATTGCCAGACCAGTG-3'
HIPK1	5'-TCCCGCTAAGCAGTGAAAAT-3'	5'-GGCAGGTATGATTCTTGCTG-3'
BCL2L11	5'-CACCAGCACCATAGAAGAA-3'	5'-ATAAGGAGCAGGCACAGA-3'
GAPDH	5'-AGGTCGGTGTGAACGGATTG-3'	5'-GGGGTCGTTGATGGCAACA-3'
U6	5'-GCTTCGGCAGCACATATACTAAAT-3'	5'-GCTTCGGCAGCACATATACTAAAT-3'

ab215203), and anti-caspase-1 (ab207802) were obtained from Abcam (Cambridge, UK), Anti-NLRP3 (#15101), anti-cleaved-caspase 8 (#9496), anti-cleaved-caspase 3 (#9664), anti-cleaved-caspase 9 (#20750), and anti-GAPDH (#5174) were obtained from CST (Boston, MA). Anti-receptor-interacting protein kinase 1 (RIPK1, PA5-20811), anti-RIPK3 (PA5-19956), anti-mixed lineage kinase domain-like protein (MLKL, PA5-43960), anti-Janus kinase 2 (JAK2, 702434), and anti-signal transducer and activator of transcription 3 (STAT3, 710077) were purchased from Invitrogen (Waltham, MA).

2.12. Statistical analysis

All experiments were conducted at least three times and the data were presented as the means \pm standard deviations. The data were analyzed using a one-way ANOVA followed by the least significance difference test. A p value $<.05$ was considered statistically significant.

3. Results

3.1. Isolation, identification, and internalization of BMSC-exos

The primary morphology of exosomes was ellipsoidal or cup-shaped as determined by transmission electron microscopy (Figure 1(A)). The size was measured by NTA and the diameter was ranged from 30 to 150 nm (Figure 1(B)). As shown in Figure 1(C), the positive markers, CD63 and TSG101 could be detected on BMSC-exos, whereas the negative marker calnexin was not detected in a western blot assay. Flow cytometry revealed that the exosomes were positive for CD73 (99.74%), CD90 (99.41%), and CD105 (99.79%), but negative for CD34 (0.11%), CD14 (0.16%), and CD45 (0.04%) (Figure 1(D)). The fluorescent dye PKH67 could stably bind to the lipid region of membranes and emit green fluorescence, thus enabling exosomes to be traced after co-culturing with cells. As shown in Figure 1(E), the marker protein PKH67, which was internalized into HK-2 cells, was successfully traced in the co-culture

medium of BMSC-exos and HK-2 cells, indicating that BMSC-exos were absorbed by HK-2 cells. In summary, BMSC-exos were isolated, identified, and absorbed and internalized by HK-2 cells.

3.2. Effect of BMSC-exos on pyroptosis induced by HG

The role of BMSC-exos in pyroptosis induced by HG was evaluated. Cell viability was notably decreased in the HG group, but the inhibitory effect was reversed by BMSC-exos (Figure 2(A)). BMSC-exo treatment markedly decreased secreted LDH, IL-1 β , and IL-18 levels in HG-treated cells (Figure 2(B,C)). MiR-30e-5p was highly expressed in the NG, MA, and HG + Exos groups, but the expression of miR-30e-5p in the HG group was decreased (Figure 2(D)). As shown in Figure 2(E,F), the level of pyroptosis was markedly decreased after BMSC-exos treatment in HG-induced cells. The expression of IL-1 β and IL-18 mRNA in the HG group was up-regulated compared with the NG and MA groups, whereas they were significantly decreased in the HG + Exos group (Figure 2(G)). In addition, Figure 2(H,I) shows that the pyroptosis markers, GSDMD-N, IL-1 β , NLRP3, and caspase-1, were markedly increased following HG treatment, but significantly decreased after BMSC-exo treatment. These results indicate that BMSC-exos ameliorate pyroptosis.

3.3. Effect of miR-30e-5p derived from BMSC-exos on pyroptosis

The function of miR-30e-5p on pyroptosis was determined in cell transfection experiments. As shown in Figure 3(A), BMSC-exos increased cell viability in HG-induced cells, but the effect was eliminated by inhibiting miR-30e-5p. Similarly, the decreased release of LDH in BMSC-exo-treated cells was reversed by knocking down miR-30e-5p (Figure 3(B)). The release of inflammatory cytokines was markedly reduced by BMSC-exos, but reversed after inhibiting miR-30e-5p (Figure 3(C)). Moreover, the pyroptosis level in the HG + Exos-

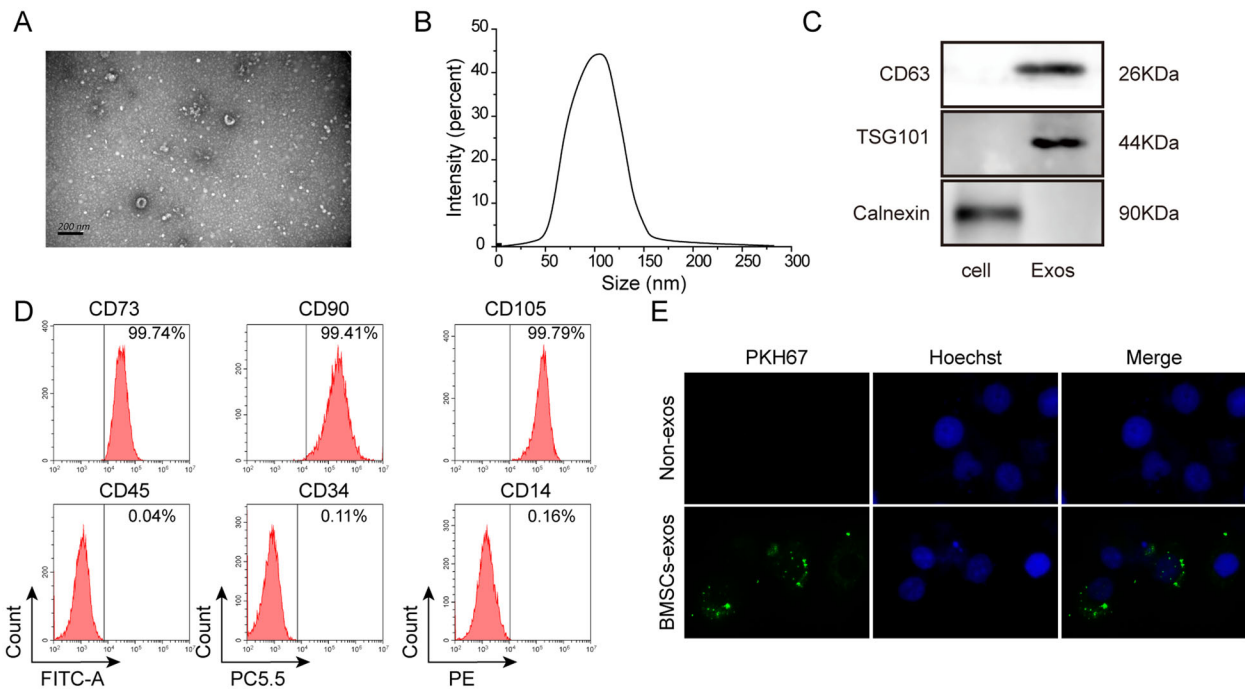


Figure 1. Isolation, identification, and internalization of exosomes derived from BMSCs. (A) Observation by transmission electron microscopy; (B) measurement of exosome size by nano-particle tracking molecule; (C) detection of BMSC-exos markers by western blot analysis; (D) detection of BMSC-exo markers by flow cytometry; (E) detection of labeled protein PKH67 by immunofluorescence assay. BMSC-exos: bone marrow MSC-derived exosomes. Three independent replications were performed.

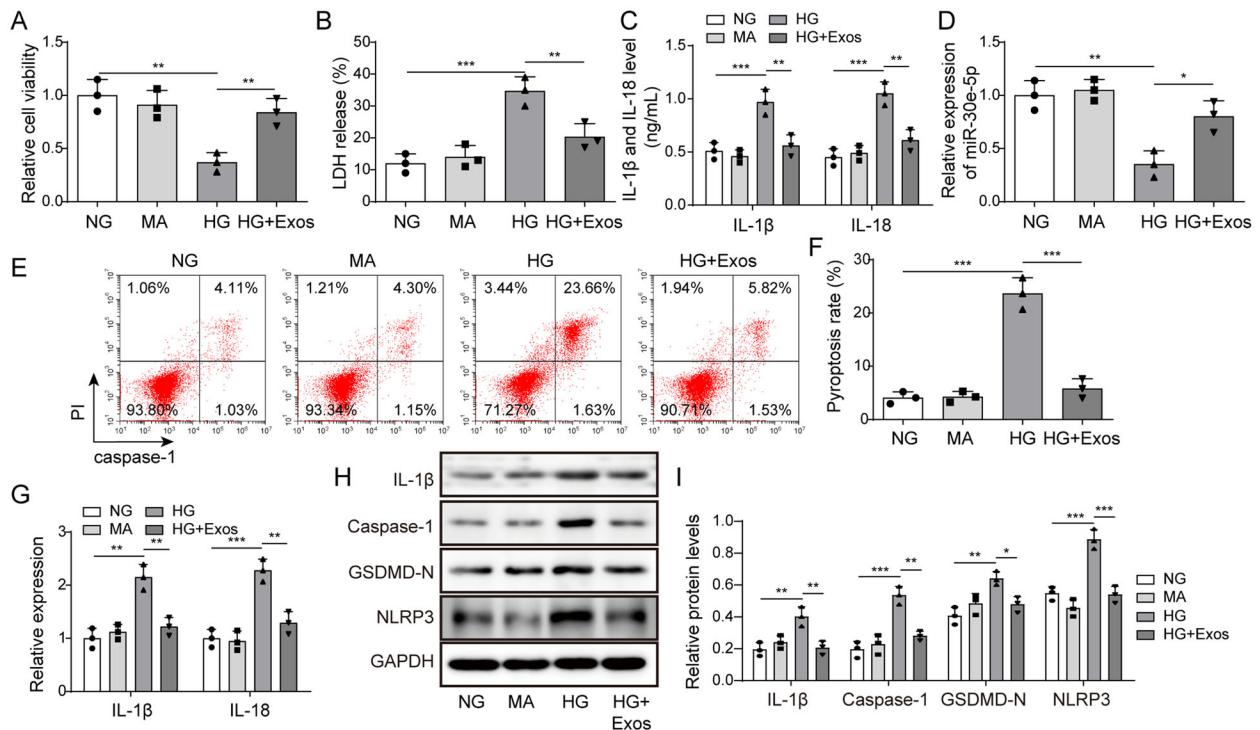


Figure 2. Effect of BMSC-exos on pyroptosis in HK-2 cells induced by HG. (A) The MTT assay was used to measure cell viability; (B) the LDH release assay was used to measure cytotoxicity; (C) IL-1 β and IL-18 levels were measured by ELISA; (D) expression of miR-30e-5p measured by RT-qPCR; (E, F) pyroptosis levels were detected by flow cytometry; (G) IL-1 β and IL-18 expression measured by qRT-PCR; (H, I) IL-1 β , caspase-1, GSDMD-N, and NLRP3 expression measured by western blot analysis. Three independent replications were performed. * $p < .05$, ** $p < .01$, and *** $p < .001$.

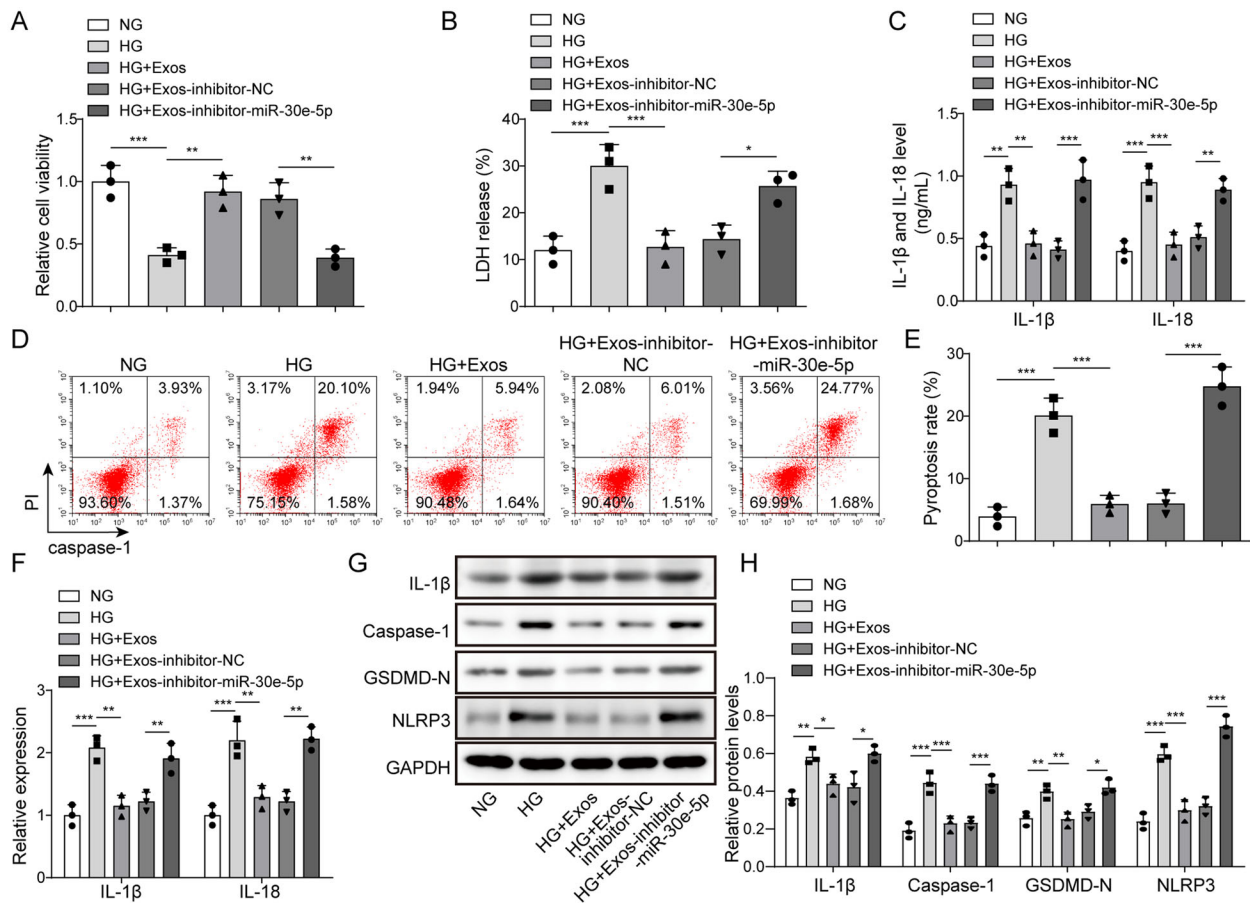


Figure 3. Effect of miR-30e-5p derived from BMSC-exos on pyroptosis. (A) The MTT assay was used to measure cell viability; (B) the LDH release assay was used to measure cytotoxicity; (C) IL-1 β and IL-18 levels were measured by ELISA; (D, E) Pyroptosis levels as detected by flow cytometry; (F) IL-1 β and IL-18 expression as measured by qRT-PCR; (G, H) IL-1 β , caspase-1, GSDMD-N, and NLRP3 expression measured by western blot analysis. Three independent replications were performed. * $p < .05$, ** $p < .01$, and *** $p < .001$.

inhibitor-miR-30e-5p group was markedly increased compared with the HG + Exos-inhibitor-NC group (Figure 3(D,E)). Moreover, the expression of IL-1 β and IL-18 was reduced by BMSC-exos in the HG treated cells and increased after miR-30e-5p inhibition (Figure 3(F)). The levels of GSDMD-N, IL-1 β , NLRP3, and caspase-1 protein were also up-regulated after inhibiting miR-30e-5p (Figure 3(G,H)). The effect of miR-30e-5p derived from BMSC-exos on HG-induced necrosis was also determined by measuring receptor-interacting protein kinase 1 (RIPK1), p-RIPK1, receptor-interacting protein kinase 3 (RIPK3), p-RIPK3, and mixed lineage kinase domain-like protein (MLKL). As shown in Figure S1A and B, HG treatment up-regulated the necrosis-related proteins, p-RIPK1, p-RIPK3, and MLKL. The increase in these proteins was significantly inhibited by BMSC-exos treatment; however, further knockdown of miR-30e-5p reversed the down-regulating effect of BMSC-exos. The effect of miR-30e-5p derived from BMSC-exos on apoptosis and JAK2/STAT3 signaling is shown in Figure S1C and D. HG treatment up-regulated apoptosis-related

proteins cleaved-caspase 8, cleaved-caspase 3, and cleaved-caspase 9, and activated the JAK2/STAT3 signal pathway. BMSC-exo treatment significantly inhibited the effect of HG treatment and further knockdown of miR-30e-5p reversed the down-regulation effect of BMSC-exos. Thus, miR-30e-5p derived from BMSC-exos exhibits a protective role in HG-induced pyroptosis, necrosis, apoptosis, and JAK2/STAT3 signaling in HK-2 cells.

3.4. Effect of miR-30e-5p overexpression or ELVAL1 knockdown on pyroptosis

As demonstrated from the above results, miR-30e-5p derived from BMSC-exos inhibited pyroptosis in HG-induced HK-2 cells. What's more, as ELVAL1 played important role in activating pyroptosis. We then investigated the effects of miR-30e-5p overexpression or ELVAL1 knockdown on HG-induced pyroptosis. The results of Figure 4(A,B) indicated that miR-30e-5p and ELVAL1 were successfully overexpressed and knocked

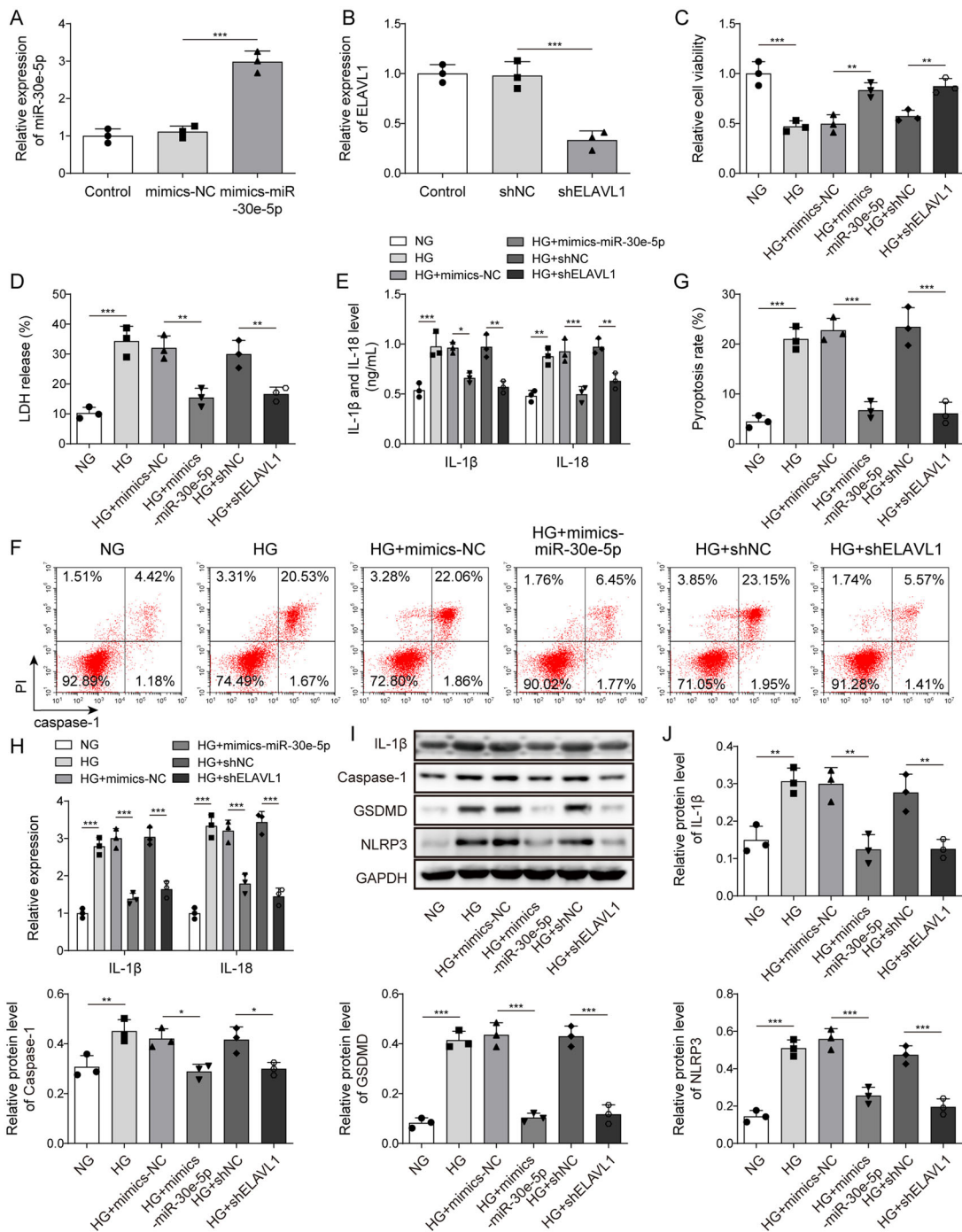


Figure 4. Effect of miR-30e-5p overexpression or ELVAL1 knockdown on HG-induced pyroptosis in HK-2 cells. (A) miR-30e-5p expression as measured by qRT-PCR; (B) ELVAL1 expression as measured by qRT-PCR; (C) the MTT assay was used to measure cell viability; (D) the LDH release assay was used to measure cytotoxicity; (E) IL-1 β and IL-18 levels were measured by ELISA; (F, G) pyroptosis levels as detected by flow cytometry; (H) IL-1 β and IL-18 expression as measured by qRT-PCR; (I, J) IL-1 β , caspase-1, GSDMD-N, and NLRP3 expression as measured by western blot analysis. Three independent replications were performed. * $p < .05$, ** $p < .01$, and *** $p < .001$.

down, respectively. Figure 4(C) shows that HG treatment inhibited cell viability; however, miR-30e-5p overexpression or ELVAL1 knockdown promoted cell viability. In addition, LDH release in the HG group was significantly higher compared with that in the NG group, whereas overexpression of miR-30e-5p or

knockdown of ELVAL1 down-regulated LDH release (Figure 4(D)). Similarly, up-regulated secretion of IL-1 β and IL-18 by HG was reversed by miR-30e-5p overexpression or ELVAL1 knockdown (Figure 4(E)). Flow cytometry revealed that HG promoted pyroptosis, which was abolished by miR-30e-5p overexpression or ELVAL1 knockdown (Figure

4(F,G). Moreover, miR-30e-5p overexpression or ELVAL1 knockdown reversed the up-regulation effect on IL-1 β and IL-18 expression induced by HG (Figure 4(H)). Finally, HG was increased the levels of pyroptosis markers, such as IL-1 β , caspase-1, GSDMD, and NLRP3; however, overexpression of miR-30e-5p or knockdown of ELVAL1 significantly down-regulated pyroptosis-related proteins (Figure 4(I,J)). These results indicated that miR-30e-5p overexpression or ELVAL1 knockdown directly inhibited pyroptosis.

3.5. Targeting effect of miR-30e-5p and ELVAL1

Using the starBase database, we found that miR-30e-5p might bind to a large number of genes including ELVAL1 (Figure 5(A)). We tested several genes that we were interested in and the results indicated that HG

treatment up-regulated ELVAL1 and methionine adenosyltransferase 2B (MAT2B) mRNA levels, down-regulated 6-phosphofructo-2-kinase/fructose-2 (PFKB2) levels, but had no effect on homeodomain interacting protein kinase 1 (HIPK1) and Bcl2-like protein 11 (BCL2L11) levels (Fig. S2). Among them, the change of ELVAL1 level was the most pronounced following HG treatment. To verify the targeting effect between miR-30e-5p and ELVAL1, a dual-luciferase reporter assay was used. We found that miR-30e-5p mimics down-regulated luciferase activity in cells when co-transfected with wt-ELVAL1 (Figure 5(B)). Thus, a mutual binding relationship existed between ELVAL1 and miR-30e-5p. In addition, qRT-PCR revealed that ELVAL1 expression was up-regulated after miR-30e-5p inhibition (Figure 5(C)). Consistently, ELVAL1 protein expression was up-regulated after

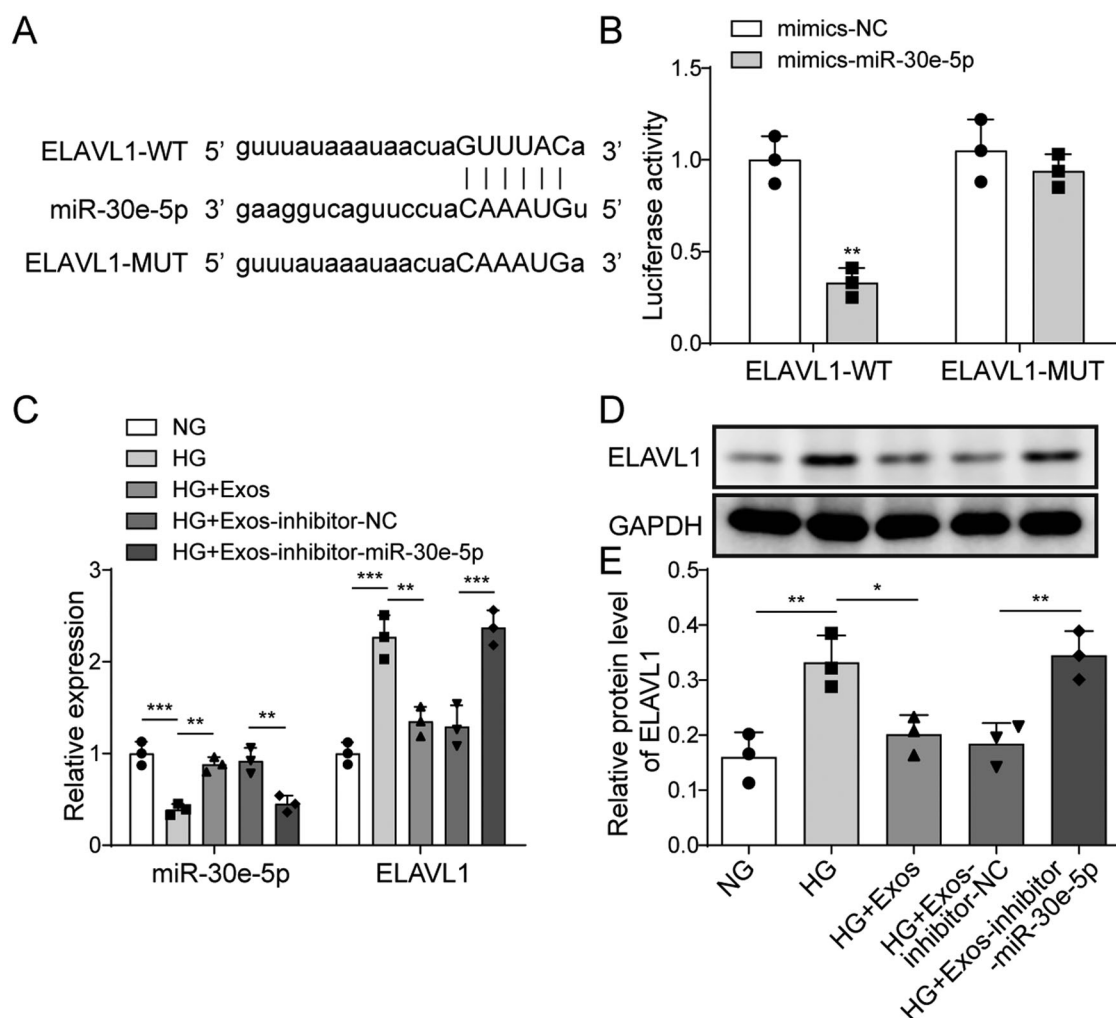


Figure 5. Targeting effect of miR-30e-5p and ELVAL1. (A) Binding site of miR-30e-5p and ELVAL1 predicted by starBase; (B) dual-luciferase reporter assay measuring the binding relationship between miR-30e-5p and ELVAL1; (C) MiR-30e-5p and ELVAL1 expression as measured by qRT-PCR; (D, E) expression of ELVAL1 as measured by western blot analysis. Three independent replications were performed. * $p < .05$, ** $p < .01$, and *** $p < .001$.

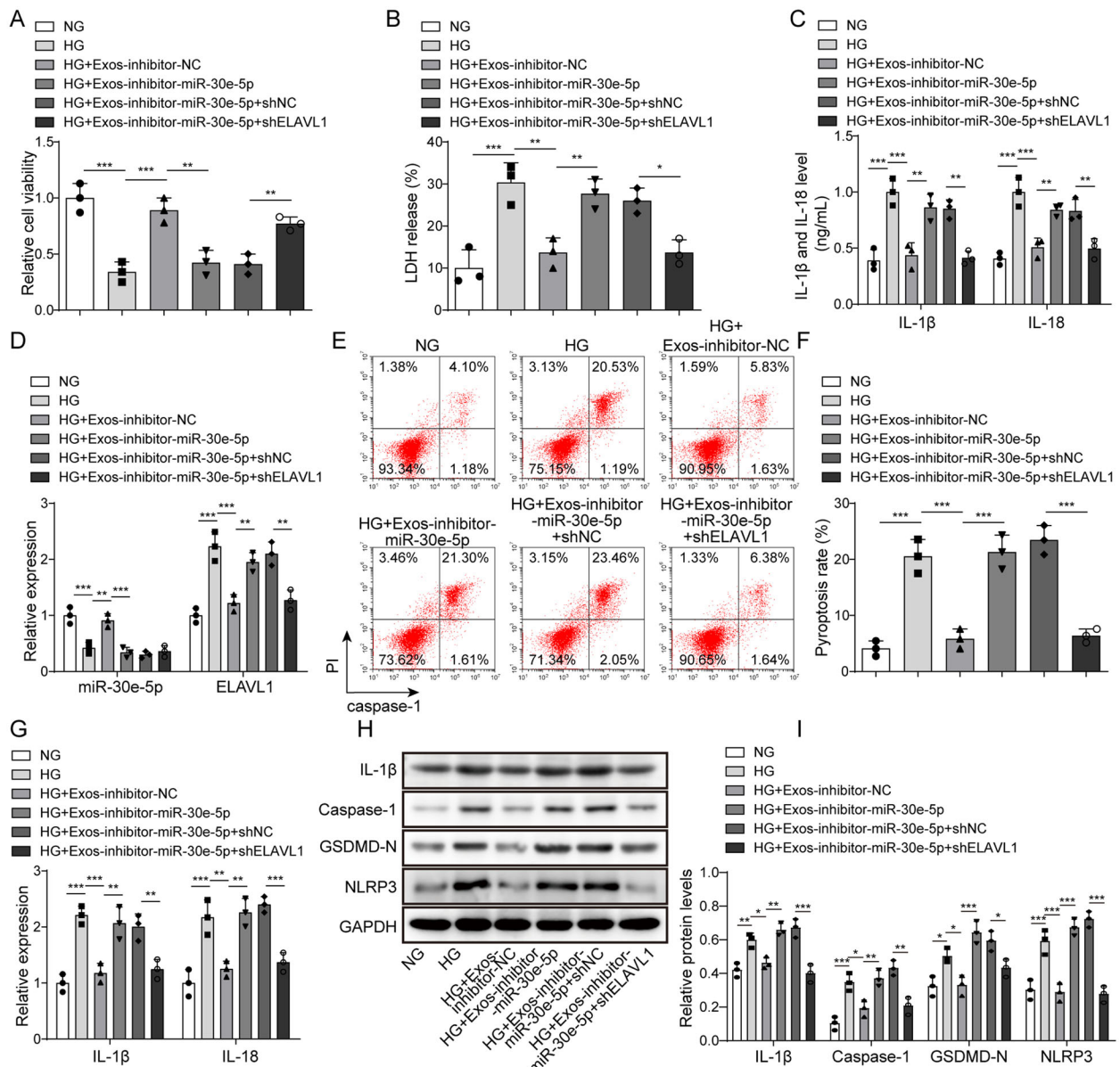


Figure 6. Effect of the miR-30e-5p/ELAVL1 axis on pyroptosis. (A) The MTT assay was used to measure cell viability; (B) the LDH release assay was used to measure cytotoxicity; (C) IL-1 β and IL-18 levels were measured by ELISA; (D) expression of miR-30e-5p and ELAVL1 as measured by qRT-PCR; (E, F) pyroptosis levels as detected by flow cytometry; (G) IL-1 β and IL-18 expression as measured by qRT-PCR; (H, I) IL-1 β , caspase-1, GSDMD-N, and NLRP3 expression as measured by western blot analysis. Three independent replications were performed. * $p < .05$, ** $p < .01$, and *** $p < .001$.

inhibiting miR-30e-5p (Figure 5(D,E)). These results suggest that ELAVL1 is a target of miR-30e-5p.

3.6. Effect of miR-30e-5p/ELAVL1 axis on pyroptosis

To confirm the effect of miR-30e-5p on pyroptosis regulated by ELAVL1, a BMSC-exo-treated diabetes model was established. Cell viability was notably decreased when inhibiting miR-30e-5p, whereas knocking down ELAVL1 reversed this effect (Figure 6(A)). The release of

LDH was increased by inhibiting miR-30e-5p, but decreased when ELAVL1 was knocked down (Figure 6(B)). In addition, the levels of secreted IL-1 β and IL-18 were increased by inhibiting miR-30e-5p and decreased again after knocking down ELAVL1 (Figure 6(C)). The level of miR-30e-5p following knockdown remained under-expressed after knocking down sh-ELAVL1. Nevertheless, the high expression of ELAVL1 caused by miR-30e-5p knockdown was down-regulated by sh-ELAVL1 (Figure 6(D)). The level of pyroptosis was increased following miR-30e-5p inhibition, whereas this

effect was reversed by knocking down ELAVL1 (Figure 6(E,F)). In addition, the promoting effects of the miR-30e-5p inhibitor on IL-1 β and IL-18 expression were dramatically reversed by ELAVL1 knockdown in the BMSC-exo-treated diabetes model cells (Figure 6(G)). Similarly, the levels of GSDMD-N, IL-1 β , NLRP3, and caspase-1 were also down-regulated in the HG + Exos-miR-30e-5p inhibitor + shELAVL1 group (Figure 6(H,I)). These results indicate that BMSC-exos may transfer miR-30e-5p into HK-2 cells, which ameliorates HG-induced pyroptosis by inhibiting ELAVL1.

4. Discussion

Both type I and type II diabetes can induce DKD [28]. However, despite extensive efforts in disease control, many patients develop not only early- and middle-stage DKD, but also end-stage chronic kidney disease. The current treatments remain limited and novel therapeutics are needed to control the progression of this disease. In the present study, BMSC-exos were shown to alleviate HG-induced HK-2 cell pyroptosis. Furthermore, BMSC-derived exosomal miR-30e-5p ameliorated HK-2 cell pyroptosis by modulating ELAVL1.

In the past few decades, MSCs have gained interest as a potential therapy for DKD. MSCs have many physiological functions including self-renewal, clone cell population generation, and multi-line differentiation [29]. As a treatment for DKD, MSCs were shown to reduce hyperglycemia and proteinuria, as well as improve renal pathological changes [30–32]. BMSC-exos can serve as vehicles to treat DKD based on their ability to exchange bioactive components and transport genetic contents [33]. In the present study, we demonstrated that BMSC-exos ameliorate pyroptosis in HG-induced HK-2 cells. Our findings provided an alternative strategy for the treatment of DKD, although the putative mechanism needs clarification.

Several studies have shown that various miRNAs are associated with DKD [31,32]. For example, miR-185 was reported to regulate the deposition of the DKD extracellular matrix by targeting TGF- β 1 [34]. The expression of miR-497 was down-regulated in the kidneys of mice with diabetes [35]. As an emerging regulator of disease progression, exosomal miRNAs are associated with a class of metabolic disorders, including diabetes and its complications [22]. Exosomal miR-215-5p derived from adipose-derived stem cells was protective against migration and inhibited podocyte damage in DKD [22]. Furthermore, exosomal miR-19b-3p derived from tubular epithelial cells inhibited inflammation to regulate DKD progression [23]. To our knowledge, miR-30e-5p

has an important role in diabetes. We demonstrated the beneficial effect of BMSC-exos on HG-induced HK-2 cell pyroptosis by transferring miR-30e-5p. This may also be helpful for using miR-30e-5p to regulate DKD.

Recent evidence has indicated that pyroptosis, a pro-inflammatory mode of programmed cell death, is involved in DKD [36]. Due to chronic exposure to diabetic substrates, pyroptosis and renal inflammation occur [37]. During the progression of pyroptosis, caspase-1 is activated by a large supramolecular complex known as the pyroptosome, which subsequently activates IL-1 β and IL-18. In the present study, HG acted as a pyroptosis inducer. LDH, IL-1 β , and IL-18 secretion was increased in the HG group as well as GSDMD-N, IL-1 β , NLRP3, and caspase-1 expression. ELAVL1, a component of the pyroptosome involved in activating pyroptosis, promotes IL-1 β and IL-18 secretion combined with caspase-1 activation [22]. Another important finding of this study was the binding relationship between ELAVL1 and miR-30e-5p. We found that miR-30e-5p could inhibit caspase-1-mediated pyroptosis in HG-induced HK-2 cells by targeting ELAVL1.

The nephron is the basic unit of kidney structure, including the renal body and connected renal tubules, which play an important role in regulating kidney function. The abnormal function of renal tubular epithelial cells is a key factor leading to DKD. Apoptosis of renal tubular epithelial cells results in abnormal renal tubular re-absorption and renal fibrosis [38]. HK-2 cells have most of the functional characteristics of normal adult renal proximal tubular cells, thus they are widely used to study renal pathology and screen therapeutic drugs *in vitro* [39]. This study focused on the regulatory mechanism of BMSC-exo-derived miR-30e-5p on HG-induced pyroptosis in HK-2 cells. The main pathological features of DKD include glomerular hypertrophy, increased production and accumulation of extracellular matrix, mesangial expansion, basement membrane thickening, glomerular follicular loss, and renal fibrosis, which leads to the progressive loss of renal function [40]. Whether miR-30e-5p affects these pathological changes in DKD *in vivo* needs to be confirmed. In addition, the glomerular filtration barrier consists of the basement membrane, the inner endothelium, and the outer podocyte epithelium. DKD was shown to be associated with necrosis of podocytes and mesangial cells [41,42]. Moreover, high glucose (HG) levels inhibited autophagy by activating the JAK/STAT pathway of podocytes, thereby preventing the effective removal of damaged proteins and organelles from the body to prevent apoptosis, and ultimately, aggravating podocyte injury and DKD progression [43]. Glomerular endothelial cell

injury is thought to contribute to the development of microalbuminuria, an early event in DKD [44]. In addition, recent studies suggested that glomerular endothelial cells may contribute to DKD through paracrine communication with other glomerular cells, such as podocytes and mesangial cells. Therefore, in addition to tubular epithelial cells, mesangial cells, and podocytes also play an important role in apoptosis, necrosis, and autophagy in DKD. However, whether BMSC-exo-derived miR-30e-5p regulates apoptosis, pyroptosis, or the necrotizing apoptosis process of other renal cells or downstream signaling warrants further investigation.

In conclusion, our findings demonstrate the ameliorative effect of BMSC-derived exosomal miR-30e-5p on HG-induced HK-2 cell pyroptosis. The underlying mechanism involves the inhibitory effect of miR-30e-5p on ELAVL1 and caspase-1-mediated pyroptosis. However, our work lacks clinical and animal experiments for further validation. In subsequent studies, we will certainly explore the effects of BMSCs-exos on the development of DKD *in vivo*. Our study is expected to provide new target and direction for the therapy of DKD.

Acknowledgements

The authors give our sincere gratitude to the reviewers for their constructive comments.

Author contributions

Ya-Ning Hao: guarantor of integrity of the entire study; Dan Niu: study concepts, study design, definition of intellectual content, manuscript preparation, and manuscript editing; Jia Lv and Wan-Hong Lu: literature research, clinical studies, data analysis, and statistical analysis; Xiao-Pei Wang: experimental studies and data acquisition; Wan-Hong Lu and Li-Yi Xie: manuscript review.

Disclosure statement

No potential conflict of interest was reported by the author(s).

Funding

This work was supported by grants from Key Research and Development Plan of Shanxi Province in China [No. 2017SF-133].

References

- [1] Moța E, Panduru MN, Popa SG, et al. Risk factors for diabetic nephropathy: intrinsic or extrinsic renal? *Rom J Intern Med.* 2009;47(4):397–401.
- [2] Toth-Manikowski S, Atta MG. Diabetic kidney disease: pathophysiology and therapeutic targets. *J Diabetes Res.* 2015;2015:697010.
- [3] Ebrahim N, Ahmed IA, Hussien NI, et al. Mesenchymal stem cell-derived exosomes ameliorated diabetic nephropathy by autophagy induction through the mTOR signaling pathway. *Cells.* 2018;7(12):226.
- [4] Khalilpourfarshbafi M, Hajiaghaalipour F, Selvarajan KK, et al. Mesenchymal stem cell-based therapies against podocyte damage in diabetic nephropathy. *Tissue Eng Regen Med.* 2017;14(3):201–210.
- [5] Keshtkar S, Azarpira N, Ghahremani MH. Mesenchymal stem cell-derived extracellular vesicles: novel frontiers in regenerative medicine. *Stem Cell Res Ther.* 2018; 9(1):63.
- [6] Zou L, Ma X, Lin S, et al. Bone marrow mesenchymal stem cell-derived exosomes protect against myocardial infarction by promoting autophagy. *Exp Ther Med.* 2019;18(4):2574–2582.
- [7] Li G, Peng H, Qian S, et al. Bone marrow-derived mesenchymal stem cells restored high-fat-fed induced hyperinsulinemia in rats at early stage of type 2 diabetes mellitus. *Cell Transplant.* 2020;29: 963689720904628.
- [8] Lee SE, Jang JE, Kim HS, et al. Mesenchymal stem cells prevent the progression of diabetic nephropathy by improving mitochondrial function in tubular epithelial cells. *Exp Mol Med.* 2019;51(7):1–14.
- [9] Xunian Z, Kalluri R. Biology and therapeutic potential of mesenchymal stem cell-derived exosomes. *Cancer Sci.* 2020;111(9):3100–3110.
- [10] Thery C, Ostrowski M, Segura E. Membrane vesicles as conveyors of immune responses. *Nat Rev Immunol.* 2009;9(8):581–593.
- [11] Corrado C, Raimondo S, Chiesi A, et al. Exosomes as intercellular signaling organelles involved in health and disease: basic science and clinical applications. *Int J Mol Sci.* 2013;14(3):5338–5366.
- [12] Bhatt K, Kato M, Natarajan R. Mini-review: emerging roles of microRNAs in the pathophysiology of renal diseases. *Am J Physiol Renal Physiol.* 2016;310(2): F109–F118.
- [13] Nascimento LRD, Domingueti CP. MicroRNAs: new biomarkers and promising therapeutic targets for diabetic kidney disease. *J Bras Nefrol.* 2019;41(3):412–422.
- [14] Hershkovitz-Rokah O, Modai S, Pasmanik-Chor M, et al. MiR-30e induces apoptosis and sensitizes K562 cells to imatinib treatment via regulation of the BCR-ABL protein. *Cancer Lett.* 2015;356(2 Pt B):597–605.
- [15] Mao J, Hu X, Pang P, et al. miR-30e acts as a tumor suppressor in hepatocellular carcinoma partly via JAK1/STAT3 pathway. *Oncol Rep.* 2017;38(1):393–401.
- [16] Laudato S, Patil N, Abba ML, et al. P53-induced miR-30e-5p inhibits colorectal cancer invasion and metastasis by targeting ITGA6 and ITGB1. *Int J Cancer.* 2017; 141(9):1879–1890.
- [17] Wang Y, Zheng ZJ, Jia YJ, et al. Role of p53/miR-155-5p/sirt1 loop in renal tubular injury of diabetic kidney disease. *J Transl Med.* 2018;16(1):146.
- [18] Delić D, Eisele C, Schmid R, et al. Urinary exosomal miRNA signature in type II diabetic nephropathy patients. *PLOS One.* 2016;11(3):e0150154.

- [19] Coll NS, Epple P, Dangl JL. Programmed cell death in the plant immune system. *Cell Death Differ.* 2011; 18(8):1247–1256.
- [20] Bergsbaken T, Fink SL, Cookson BT. Pyroptosis: host cell death and inflammation. *Nat Rev Microbiol.* 2009; 7(2):99–109.
- [21] Frank D, Vince JE. Pyroptosis versus necroptosis: similarities, differences, and crosstalk. *Cell Death Differ.* 2019;26(1):99–114.
- [22] Li X, Zeng L, Cao C, et al. Long noncoding RNA MALAT1 regulates renal tubular epithelial pyroptosis by modulated miR-23c targeting of ELAVL1 in diabetic nephropathy. *Exp Cell Res.* 2017;350(2):327–335.
- [23] Shi Q, Lee DY, Feliers D, et al. Interplay between RNA-binding protein HuR and Nox4 as a novel therapeutic target in diabetic kidney disease. *Mol Metab.* 2020;36: 100968.
- [24] Fan J, Xie K, Wang L, et al. Roles of inflammasomes in inflammatory kidney diseases. *Mediators Inflamm.* 2019;2019:2923072.
- [25] Zhang H, Wang Z. Effect and regulation of the NLRP3 inflammasome during renal fibrosis. *Front Cell Dev Biol.* 2019;7:379.
- [26] Qiu Z, Zhong Z, Zhang Y, et al. Human umbilical cord mesenchymal stem cell-derived exosomal miR-335-5p attenuates the inflammation and tubular epithelial-myofibroblast transdifferentiation of renal tubular epithelial cells by reducing ADAM19 protein levels. *Stem Cell Res Ther.* 2022;13(1):373.
- [27] Li D, Zhang D, Tang B, et al. Exosomes from human umbilical cord mesenchymal stem cells reduce damage from oxidative stress and the epithelial-mesenchymal transition in renal epithelial cells exposed to oxalate and calcium oxalate monohydrate. *Stem Cells Int.* 2019;2019:6935806.
- [28] Thomas MC, Cooper ME, Zimmet P. Changing epidemiology of type 2 diabetes mellitus and associated chronic kidney disease. *Nat Rev Nephrol.* 2016;12(2): 73–81.
- [29] Konari N, Nagaishi K, Kikuchi S, et al. Mitochondria transfer from mesenchymal stem cells structurally and functionally repairs renal proximal tubular epithelial cells in diabetic nephropathy in vivo. *Sci Rep.* 2019; 9(1):5184.
- [30] Lee RH, Seo MJ, Reger RL, et al. Multipotent stromal cells from human marrow home to and promote repair of pancreatic islets and renal glomeruli in diabetic NOD/scid mice. *Proc Natl Acad Sci U S A.* 2006; 103(46):17438–17443.
- [31] Lv S, Cheng J, Sun A, et al. Mesenchymal stem cells transplantation ameliorates glomerular injury in streptozotocin-induced diabetic nephropathy in rats via inhibiting oxidative stress. *Diabetes Res Clin Pract.* 2014;104(1):143–154.
- [32] Zhou H, Tian HM, Long Y, et al. Mesenchymal stem cells transplantation mildly ameliorates experimental diabetic nephropathy in rats. *Chin Med J.* 2009; 122(21):2573–2579.
- [33] Xiang E, Han B, Zhang Q, et al. Human umbilical cord-derived mesenchymal stem cells prevent the progression of early diabetic nephropathy through inhibiting inflammation and fibrosis. *Stem Cell Res Ther.* 2020; 11(1):336.
- [34] Hu W, Han Q, Zhao L, et al. Circular RNA circRNA_15698 aggravates the extracellular matrix of diabetic nephropathy mesangial cells via miR-185/TGF-beta1. *J Cell Physiol.* 2019;234(2):1469–1476.
- [35] Ban E, Jeong S, Park M, et al. Accelerated wound healing in diabetic mice by miRNA-497 and its anti-inflammatory activity. *Biomed Pharmacother.* 2020;121: 109613.
- [36] Mamun A, Ara Mimi A, Wu A, et al. Pyroptosis in diabetic nephropathy. *Clin Chim Acta.* 2021;523:131–143.
- [37] Lin J, Cheng A, Cheng K, et al. New insights into the mechanisms of pyroptosis and implications for diabetic kidney disease. *Int J Mol Sci.* 2020;21(19):7057.
- [38] Wang H, Huang S, Hu T, et al. Circ_0000064 promotes high glucose-induced renal tubular epithelial cells injury to facilitate diabetic nephropathy progression through miR-532-3p/ROCK1 axis. *BMC Endocr Disord.* 2022;22(1):67.
- [39] Lin CY, Lin YC, Paul CR, et al. Isoliquiritigenin ameliorates advanced glycation end-products toxicity on renal proximal tubular epithelial cells. *Environ Toxicol.* 2022;37(8):2096–2102.
- [40] Kim D, Nam GY, Seo E, et al. Inhibition of ChREBP ubiquitination via the ROS/Akt-dependent downregulation of Smurf2 contributes to lysophosphatidic acid-induced fibrosis in renal mesangial cells. *J Biomed Sci.* 2022;29(1):31.
- [41] Ma T, Li X, Zhu Y, et al. Excessive activation of notch signaling in macrophages promote kidney inflammation, fibrosis, and necroptosis. *Front Immunol.* 2022; 13:835879.
- [42] Xu Y, Gao H, Hu Y, et al. High glucose-induced apoptosis and necroptosis in podocytes is regulated by UCHL1 via RIPK1/RIPK3 pathway. *Exp Cell Res.* 2019; 382(2):111463.
- [43] Chen D, Liu Y, Chen J, et al. JAK/STAT pathway promotes the progression of diabetic kidney disease via autophagy in podocytes. *Eur J Pharmacol.* 2021;902: 174121.
- [44] Fu J, Lee K, Chuang PY, et al. Glomerular endothelial cell injury and cross talk in diabetic kidney disease. *Am J Physiol Renal Physiol.* 2015;308(4):F287–F297.